Security Classification

DOCUMENT CONTROL DATA - R & D

(Security classification of title, body of abstract and indexing annotation must be entered when the overall report is classified)

1. ORIGINATING ACTIVITY (Corporate author)	2a. REPORT SECURITY CLASSIFICATION
Naval Research Laboratory Washington, D.C. 20390	Unclassified
	2b. GROUP

3. REPORT TITLE

THE FLOW STRENGTH DEPENDENCE ON TEMPERATURE AND STRAIN RATE IN LOW-CARBON IRON ALLOYS

4. DESCRIPTIVE NOTES (Type of report and inclusive dates)

An interim report on one phase of the work; work is continuing.

5. AUTHOR(S) (First name, middle initial, last name)

A.R. Cox and L.R. Hettche

6. REPORT DATE	7a. TOTAL NO. OF PAGES	7b. NO. OF REFS
August 4, 1971	28	40

8a. CONTRACT OR GRANT NO.	9a. ORIGINATOR'S REPORT NUMBER(S)
NRL Problem F01-03A b. PROJECT NO. RR 009-03-45-5450 c. d.	NRL Report 7283 9b. OTHER REPORT NO(S) (Any other numbers that may be assigned this report)

10. DISTRIBUTION STATEMENT

Approved for public release; distribution unlimited.

11. SUPPLEMENTARY NOTES	12. SPONSORING MILITARY ACTIVITY
	Department of the Navy (Office of Naval Research) Arlington, Va. 22217

13. ABSTRACT

The flow strengths of a series of iron-carbon alloys, containing silicon, manganese, nickel, and phosphorus, were measured over the strain-rate range 10^{-3} to 10 sec^{-1}. At 24°C all four elements reduced the strain-rate sensitivity of the base alloy (0.02 wt-% C) but, with the exception of the combined addition of silicon and manganese, had little effect at -195°C. At a strain rate of 2 sec^{-1}, the thermal component of the strength was reduced by the alloying elements. This reduction was sufficient in the carbon, nickel, and phosphorus alloys to make their total strength less than that of the unalloyed iron at some temperatures. These results are discussed in terms of the current solution-softening models.

DD FORM 1 NOV 65 1473 (PAGE 1)

S/N 0101-807-6801

Security Classification

14. KEY WORDS	LINK A		LINK B		LINK C	
	ROLE	WT	ROLE	WT	ROLE	WT
Low-carbon iron alloy Isothermal flow strength Strain-rate sensitivity Tensile instability strain Solution softening Interstitial-induced cross slip						

CONTENTS

ABSTRACT

The flow strengths of a series of iron-carbon alloys, containing silicon, manganese, nickel and phosphorus, were measured over the strain-rate range 10^{-3} to 10 sec^{-1}. At 24°C all four elements reduced the strain-rate sensitivity of the base alloy (0.02 wt-% C) but, with the exception of the combined addition of silicon and manganese, had little effect at -195°C. At a strain rate of 2 sec^{-1}, the thermal component of the strength was reduced by the alloying elements. This reduction was sufficient in the carbon, nickel, and phosphorus alloys to make their total strength less than that of the unalloyed iron at some temperatures. These results are discussed in terms of the current solution-softening models.

PROBLEM STATUS

This is an interim report on this program; work is continuing on this phase of the problem.

AUTHORIZATION

NRL Problem F01-03A
Project RR 009-03-45-5450

Manuscript submitted March 24 1971.

THE FLOW-STRENGTH DEPENDENCE ON TEMPERATURE AND STRAIN RATE IN LOW-CARBON IRON ALLOYS

INTRODUCTION

In any engineering design one of the prime requisites, once the problems of salability and financial profitability have been resolved, is to maximize the material toughness for the strength level required. Such a demand assures the designer a factor of safety against unexpected impact loading, and experience has shown this to be a useful asset.

Designing for toughness quantitatively is difficult and was virtually impossible until the advent of recent developments in linear elastic fracture mechanics (LEFM). Even now, the limitations are probably more evident than the possibilities. Prevoius designers have relied on the toughness data supplied by the manufacturer, combined with their own experience of adequate toughness for a particular task in hand. In the majority of applications this philosophy has proved satisfactory. Shortcomings in this approach do become evident when restrictions are placed on weight, as in aerospace and military hardware, where the components operate under high working stresses in adverse environments. For these conditions, the material is selected after completing specific tests simulating the operating environment, but the very nature of the tests allow their results to relate only to specific conditions and not to general behavior. These tests represent a considerable investment in time and money; consequently, there is continual research into identifying a toughness parameter applicable to most situations.

Currently, no general method is available for determining this parameter, though the ideal is nearing realization for some materials which break in a macroscopically brittle manner and to which LEFM is applicable. Success has been achieved in using these concepts to establish the critical flaw sizes that can be tolerated for given stress levels, but the method is mainly restricted to high-strength alloys. This limitation is a consequence of the elastic constraint required at the crack tip since, if plastic flow is excessive, the assumptions made in the elastic analysis are not satisfied. In lower-strength alloys the elastic constraint condition may be satisfied if the section size is sufficiently large.

Concurrent with the mechanics approach to fracture, the macroscopic structure of metals and alloys has received generous attention, and some useful correlations have been obtained between the metallurgical structure and fracture behavior. Krafft (1) has shown that the distribution of nonmetallic inclusions is a significant factor controlling the toughness and has developed a model relating the crack tip separation process to the fracture toughness parameters. Models which attempt to make this correlation are rare; most investigators concentrate on the phenomenological aspects of fracture as evidenced by the work on the influence of twins (2,3), the cracking of carbides (4,5), studies of void nucleation and growth (6), and models for crack nucleation (7,8).

Different approaches are used because the complexity of the separation processes requires that the particular facets be isolated and the details recognized. The principal modes of metal rupture are recognized, but what constitutes the optimum matrix, carbide distribution, or dislocation configuration necessary for maximum toughness have yet to be defined. There is agreement on the influence of grain size and cleanliness, i.e., the smaller the grain size and the fewer inclusions, the tougher the material.

NOTE: A. R. Cox is an exchange scientist from Royal Armament Research and Development Establishment, United Kingdom.

One of the problems encountered when relating the metallurgical structure to the toughness is the difficulty in obtaining quantitative fracture data which can be related to the separation processes. Metallurgical structures have been equally unpredictable, with dissimilar properties being obtained from structures which look much the same, even in high-resolution electron microscopes.

The apparent insensitivity of the toughness to the carbide dispersion, on occasions, has lead the authors to examine the matrixes found in alloy steels with the object of identifying the matrix properties which confer maximum toughness. Krafft et al. (9) have shown that the strain at tensile instability is a major parameter influencing toughness. Therefore, the purpose of the first part of the present program was to determine the tensile flow properties and hence the instability strains of a series of iron alloys. Six iron alloys were made, one containing as low an interstitial level as could be made in the laboratory with the available equipment, 0.002 wt-% C, and five irons containing 0.02 wt-% C. This latter carbon level was adopted to reproduce the carbon remaining in solution after quenching and tempering a low-alloy steel between 600° and 700°C. To three of these irons, either nickel, silicon, or silicon and manganese were added to further reproduce typical iron matrixes. Phosphorus was added to one alloy, primarily to facilitate intergranular separation and to show the influence of a change in fracture mode. All the elements added were those commonly found in steels and in quantities sufficient to produce significant changes in the mechanical properties. The plastic flow properties of the alloys were determined from compression tests at the constant strain rates 10^{-3} to 10 sec^{-1} and at temperatures between -195° and 121°C under isothermal conditions. As discussed subsequently, this condition is necessary if the flow properties are to be relevant to the stress state existing at the crack tip. In this report, however, the isothermal value of the test is not significant because the strengths presented are for 4% plastic strain, a level at which the thermal softening is negligible, but it is important when measuring flow strength and the work-hardening rates at higher strain levels.

MATERIALS

The six iron alloys given in Table 1 were melted and cast as 50-lb ingots in an Ajax induction furnace, followed by forging the carbon and alloy iron ingots to 1.5-in. and 1-in. square bars, respectively, at 1100°C. Subsequent reduction to 0.4-by-0.8-in. bars was started at 550°C, and the forging was completed in the range 300° to 350°C. This working represented 75% and 55% reduction for the carbon and alloy irons, respectively, and produced cold-worked structures which were subsequently recrystallized to grain sizes in the range 5 to 8 ASTM. The details of the recrystallization treatments are given in Table 1. All heat treatments were in vacuo on the finished test pieces to minimize the effect of machine-induced surface stresses which are reported to influence the properties (10). After recrystallization, the test pieces were either water quenched and aged at

Table 1
Composition, Recrystallization Treatment, and Grain Size

Alloy (nominal composition)	Composition (wt-%)								N_2 (ppm)	O_2 (ppm)	Recrystallization Heat Treatment	Grain Size ASTM
	C	Si	Mn	Cr	Ni	P	S	Ti				
Fe-0.002 C	0.002	0.004	0.005	0.01	0.06	—	—	<0.1	19	95	30 min @ 600°C	6-8
Fe-0.02 C	0.026	0.006	0.005	0.008	0.08	0.004	0.004	<0.004	9	22	30 min @ 700°C	6-7
Fe-2 Si	0.034	1.96	0.009	0.01	0.05	0.001	0.004	<0.004	10	26	7 hr @ 810°C	5-7
Fe-2 Si-1 Mn	0.032	1.99	0.91	0.01	0.05	0.001	0.004	<0.004	12	23	1 hr @ 700°C	7-8
Fe-3 Ni	0.020	0.013	0.005	0.05	2.84	0.003	0.005	0.004	10	30	1 hr @ 770°C	6-7
Fe-P	0.028	0.011	0.005	0.04	0.05	0.25	0.003	<0.004	10	20	30 min @ 770°C	6-7

ambient temperature for 2 or 3 months, water quenched and stored in liquid nitrogen prior to testing, or furnace cooled.

TEST PROCEDURE FOR DETERMINING ISOTHERMAL FLOW PROPERTIES

To determine the strain rate and temperature sensitivity of the localized deformation at the leading edge of a sharp crack, a distinction must be made between the initiation and propagation stages of the crack growth process. As reasoned by Krafft and Eftis (11) and Krafft and Irwin (12), the time for quenching the small elastic zone at a crack tip is several orders of magnitude faster than the most rapid of impact loadings. Thus, during the initiation stages, the deformation preceding crack growth is an isothermal process. Conversely, the strain rate associated with a running crack is several orders of magnitude greater than the initiation value, and the thermal state is adiabatic.

In a conventional tension or compression test, thermal conditions also depend on the rate of loading. A standard-size specimen retains its heat of deformation for strain rates above 0.1 sec^{-1}. The corresponding temperature rise reduces the flow stress required to maintain a constant rate of straining—a decrease in the effective work-hardening rate $d\sigma/d\epsilon$. The effect of thermal softening is most pronounced at low temperature due to the accompanying decrease in specific heat. To simulate the fully quenched condition over a range of strain rates and temperatures, Krafft (1) has developed a test procedure in which a compression plug is deformed in a series of strain-quench steps. The loading anvil is abruptly arrested when a rigid platform is engaged. The magnitude of the strain increment is controlled by the distance the specimen protrudes above the platform. Before the next strain increment is applied, the anvil is retracted, and the specimen is quenched and repositioned. The isothermal stress-strain relationship is defined by plotting the total strain after each step versus the yield stress on subsequent loading. A more complete description of this testing procedure is available in recent publications (1,9,11).

The compression plugs (0.4375 in. long by 0.25 in. diameter) of the iron alloys were deformed in eight to ten steps using a Krafft-Hahn dynamic loader. The load was measured by a strain-gage-instrumented loading anvil which was calibrated from a standard cell. The deflection of the specimen was monitored by two flectural cantilever beams, also instrumented with strain gages to track the crosshead displacement. A typical load-displacement oscillograph and its isothermal stress-strain construction are shown in Fig. 1. Tests were performed at a near constant strain rate over the range 10^{-4} to 15 sec^{-1}. The strain rate is measured during the fouth step, which is the 8 to 10% strain increment, by superimposing time marks on the load-deflection trace (Fig. 1). All temperatures were measured by copper-constantan thermocouple with the test piece temperature within ±3°C of the indicated temperature. Test temperatures were controlled by blowing nitrogen gas or hot air through the test rig. Considering the various sources of error (e.g., calibration, instrumentation, and temperature variations) as accumulative, the stress, strain, and strain-rate measurements are conservatively estimated to be within 5% of true values and reproducible to within 2%.

From the compression curve the tensile curve is derived using the method described in the Appendix and the 4% flow strengths determined. To illustrate the difference between the adiabatic and isothermal flow curves, the 0.002% C iron was tested under both conditions at a strain rate ($\dot{\epsilon}$) of 2 sec^{-1}. At room temperature (24°C) the flow curves are similar for the two conditions, Fig. 2, with limited thermal softening, but softening is evident at -140°C and -195°C. After 4% strain, the strengths are comparable, but at the 8% strain the strength under isothermal testing is 10 ksi greater than for adiabatic testing and the difference continues to increase with strain.

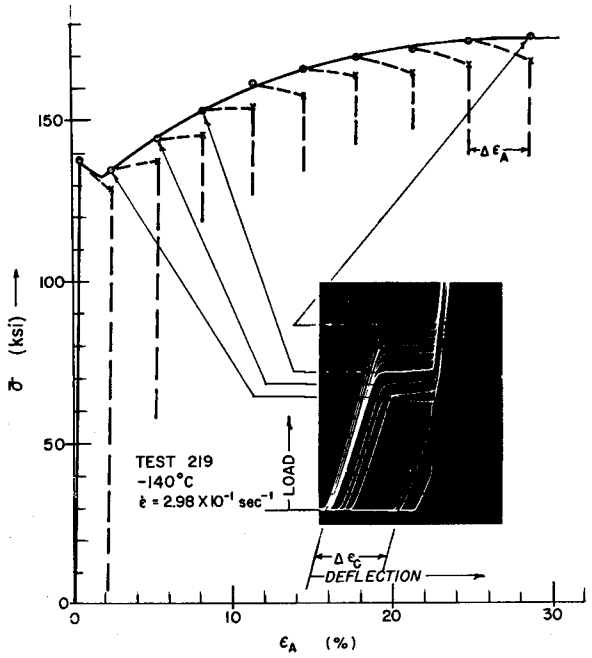

Fig. 1 - Oscilloscope record of compressive load versus deflection in 10 incremental straining steps. The isothermal (σ - ϵ) curve (solid line) is derived by plotting total strain after each increment versus yield stress on subsequent loading. The dotted line indicates the thermal softening effect in each loading cycle.

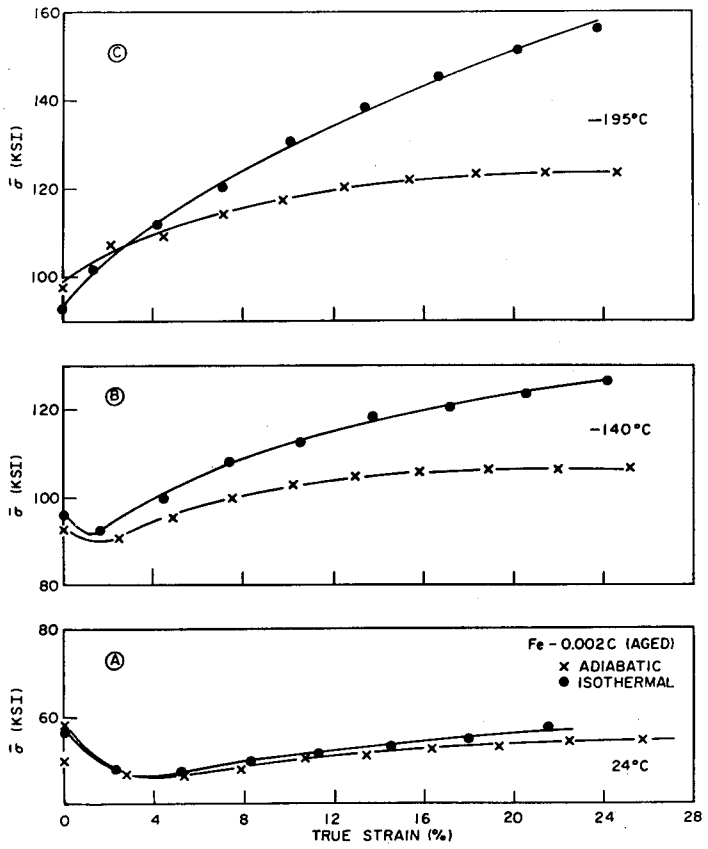

Fig. 2 - Comparison of adiabatic and isothermal stress-strain curves for the 0.002% carbon iron in the aged condition at a strain rate of 2 sec^{-1}

OPTICAL AND ELECTRON METALLOGRAPHY OF THE ALLOYS

In the cold-worked and annealed state the alloys were recrystallized, and with the exception of the nickel alloy all structures were composed of the conventional straight-sided, equiaxed grains. When nickel was present, the grains lost their angular shape, and boundaries showed considerable curvature, suggesting that the grain boundary energies were modified. Both phosphorus and nickel additions produced composition banding due to segregation in the original ingot, but this has previously been found to have a negligible effect on the flow properties (13).

Examination of the alloys in the electron microscope after quenching and aging for 2 months at room temperature showed all the alloys, with the exception of the 0.002% C iron, to be unstable. This alloy had a low dislocation density and a few second-phase particles, Fig. 3a. The carbides present in the 0.02% C alloys were assumed to be ϵ carbide on the basis of the aging treatment and studies of comparable systems (14,15).

The alloying elements modified the carbide nucleation and growth kinetics and the structures differed considerably. In the plain 0.02% C iron the carbide precipitated on the dislocations with no evidence of grain boundary carbide. Figure 3b shows that at the recrystallization temperature all the carbon was in solution. Silicon modified the iron alloy to give a dense dispersion of homogeneously nucleated coherent carbide particles, Fig. 3c, but when manganese was present with the silicon the precipitation was considerably reduced, Fig. 3d.

In contrast to the effects of silicon, nickel promoted heterogeneous nucleation of the carbides on the dislocations, Fig. 3e, with little evidence of strain fields around the particles, although a significant strength increase accompanied the aging. Phosphorus produced changes on the iron alloy similar to those effected by silicon, with dense homogeneously nucleated carbides growing rapidly and showing strain fields, Fig. 3f. An unidentified thin film of the second phase was along some boundaries, but investigations on the embrittling effects of phosphorus indicated it to be some form of a phosphorus-rich compound (16).

At room temperature all the alloys deformed by slip, with slip and twinning occurring at -195°C. For temperatures in the 24°C to -195°C range at $\dot{\epsilon} = 2$ sec^{-1}, deformation always involved some slip, although below -29°C deformation resulted from twinning in addition to slip in the 0.002% C and 0.02% C irons. The higher-carbon alloy showed a reduced twin frequency in comparison to the lower-carbon alloys. Both silicon and nickel suppressed the formation of twins, which were first observed after testing at -84°C. The percentage of twinned grains in the nickel alloy was always smaller than in the silicon alloy. Phosphorus and the silicon-manganese additions also suppressed twin formation, the twins first being observed after testing at -140°C.

THE STRAIN-RATE SENSITIVITY AT 24°C AND -195°C

The 4% flow strengths $\bar{\sigma}_{0.04}$ were determined at 24°C and -195°C for the six alloys aged at ambient temperature for 2 months for constant $\dot{\epsilon}$ between 10^{-5} and 15 sec^{-1}. At room temperature the two iron-carbon alloys showed the greatest strain-rate sensitivity, $d\sigma/d\dot{\epsilon}$, the strength increasing by 20 ksi over four decades of strain rate, Fig. 4a and 4b. Reducing the temperature to -195°C increased the strength of the irons but the strain-rate sensitivity was reduced to half the room-temperature value. The different carbon contents of the two irons had little effect on the strength at -195°C, but at room temperature the higher-carbon alloy was stronger for $\dot{\epsilon} < 1$ sec^{-1}.

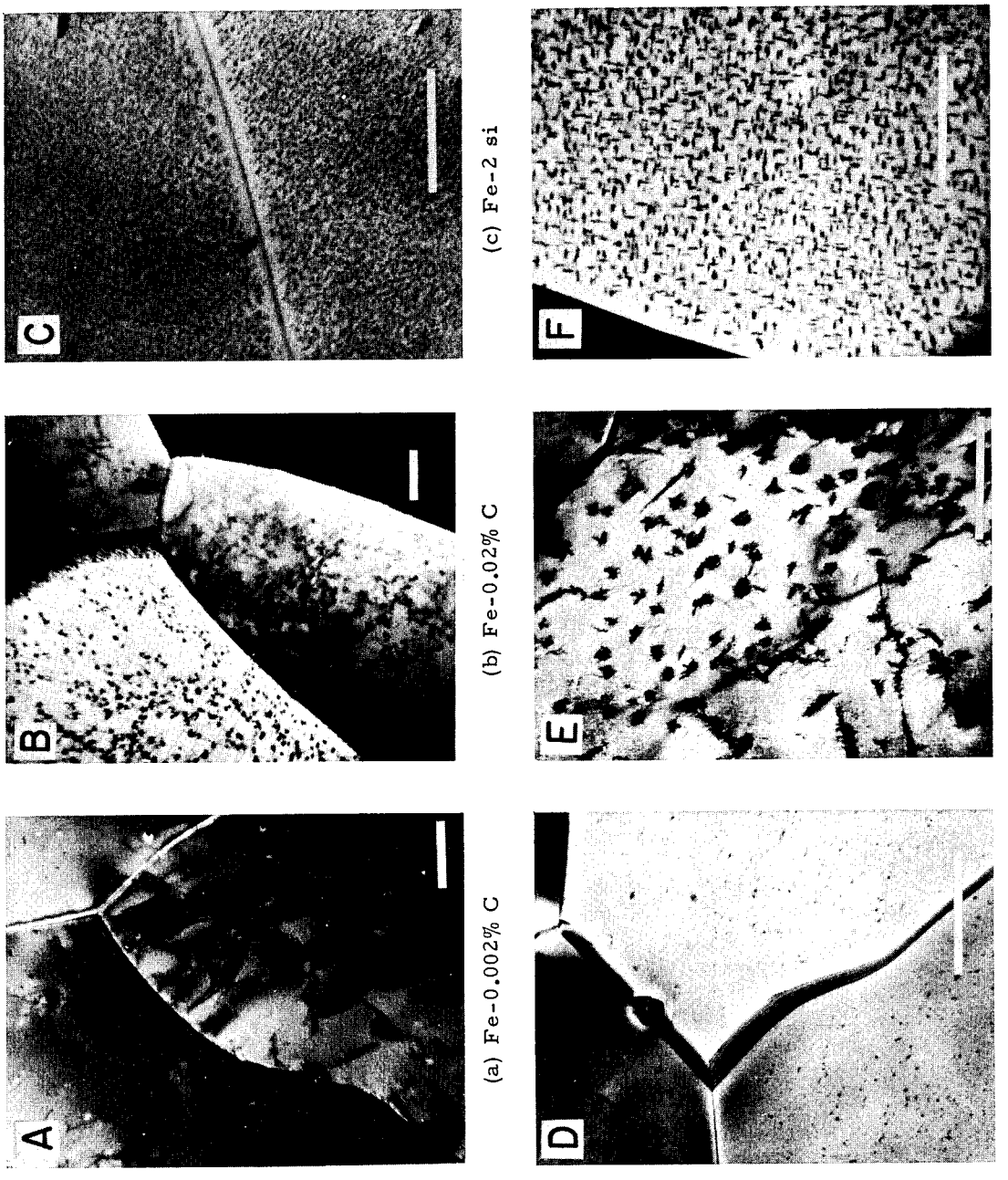

(a) Fe-0.002% C (b) Fe-0.02% C (c) Fe-2 si

(d) Fe-2 Si-1 Mn (e) Fe-3 Ni (f) Fe-0.3 P

Fig. 3 - Transmission electron micrographs of the six iron alloys aged 2 months at 24°C. Scale line is 1 micron.

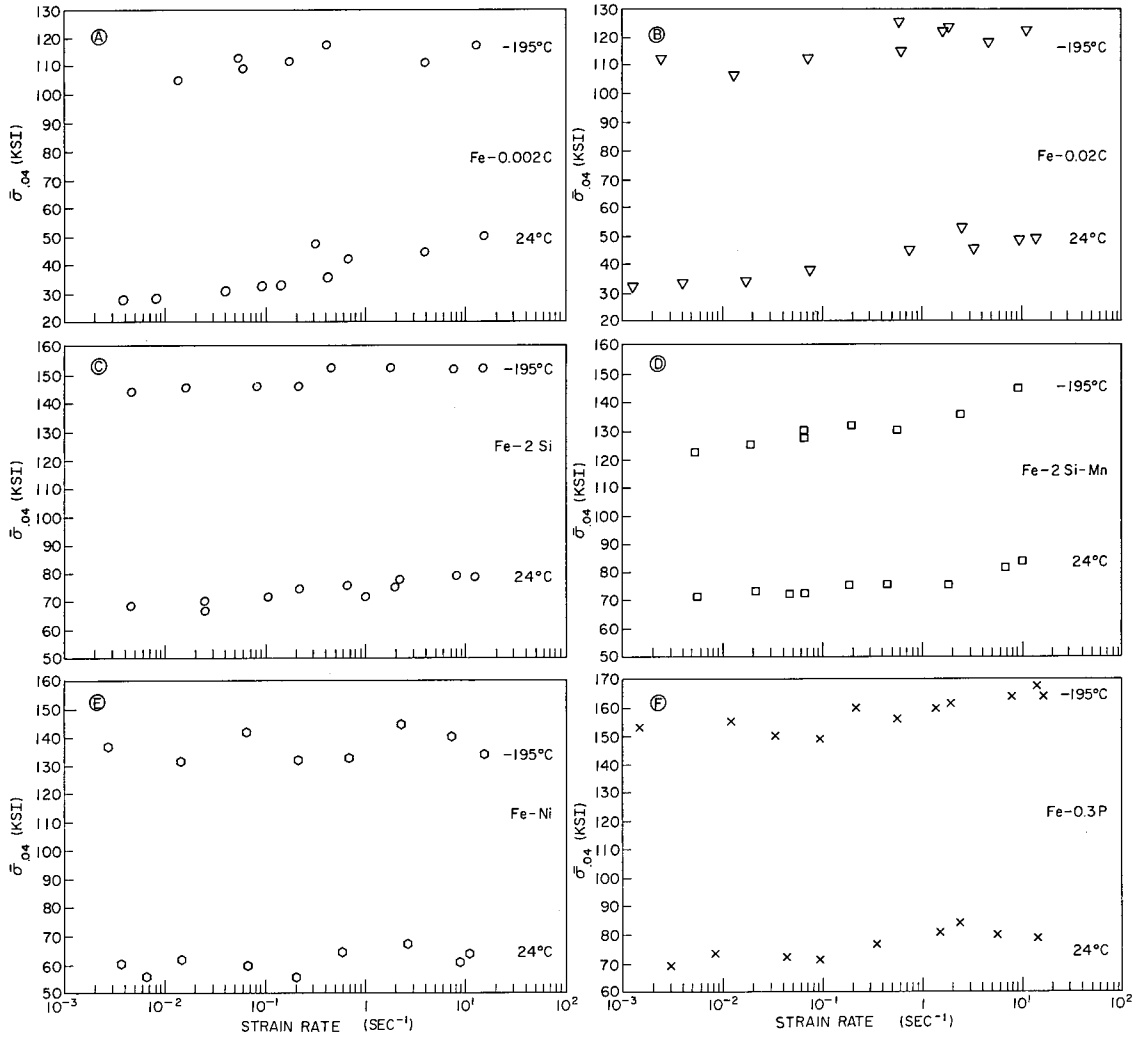

Fig. 4 - Strain-rate sensitivity of the six iron alloys (aged 2 months at 24°C) at -195°C and 24°C

The addition of 2% silicon increased the strength at 24°C and -195°C but reduced the strain-rate sensitivity, Fig. 4c. Over four strain-rate decades the flow stress increased by 10 ksi at 24°C with a similar increase shown at -195°C. At room temperature, manganese had a negligible effect on the strength or strain-rate sensitivity of the silicon iron alloy, but at -195°C the strength was reduced for $\dot{\epsilon} < 10$ sec^{-1} and the strain-rate sensitivity was increased, Fig. 4d. This increase in the strain-rate sensitivity was such that at $\dot{\epsilon} \approx 10^{-3}$ sec^{-1} the strength of the silicon-manganese alloy was 40 ksi less than the strength of the silicon alloy compared with a difference of 10 ksi at 10 sec^{-1}.

In the nickel alloy the strain-rate sensitivity cannot be so readily generalized because the data do not fall on a monotonic curve, Fig. 4e. The data can either be interpreted as fluctuating about a mean, with the scatter representing experimental error (the conventional interpretation), or, alternatively, the variation observed may be a manifestation of the "rate spectrum" effects observed in alloy steels by Krafft et al. (9) and Hettche (17). If the former interpretation is correct, the strain-rate sensitivity at both temperatures is negligible, while if the latter occurs, the local strain-rate sensitivity, over specific strain-rate ranges, is large and may be either positive or negative. With phosphorus the

strength at 24°C and -195°C increased by 10 ksi over the strain-rate range, but the increase was not uniform and the alloy was essentially strain-rate insensitive between 10^{-3} to 10^{-1} and 1 to 15 sec^{-1}; the strength increase occurred in the range 10^{-1} to 1 sec^{-1}, Fig. 4f. A discontinuous strain-rate sensitivity was also shown by the silicon alloy at -195°C. Similar stepwise dependence of strength has previously been reported for low-alloy steels (9).

A comparison of the alloy strengths in Fig. 5a shows that at 24°C the phosphorus, silicon, and silicon-manganese alloys are comparable and substantially stronger than the nickel alloy, the difference increasing with strain rate because the mean strength of the nickel-iron alloy is strain-rate insensitive. The nickel alloy is 30 ksi stronger than the carbon-iron alloys at $\dot{\epsilon} = 10^{-3}$ sec^{-1}, but the difference decreases to 15 ksi at $\dot{\epsilon} = 10$ sec^{-1} because of the high strain-rate sensitivity of the carbon-iron alloys.

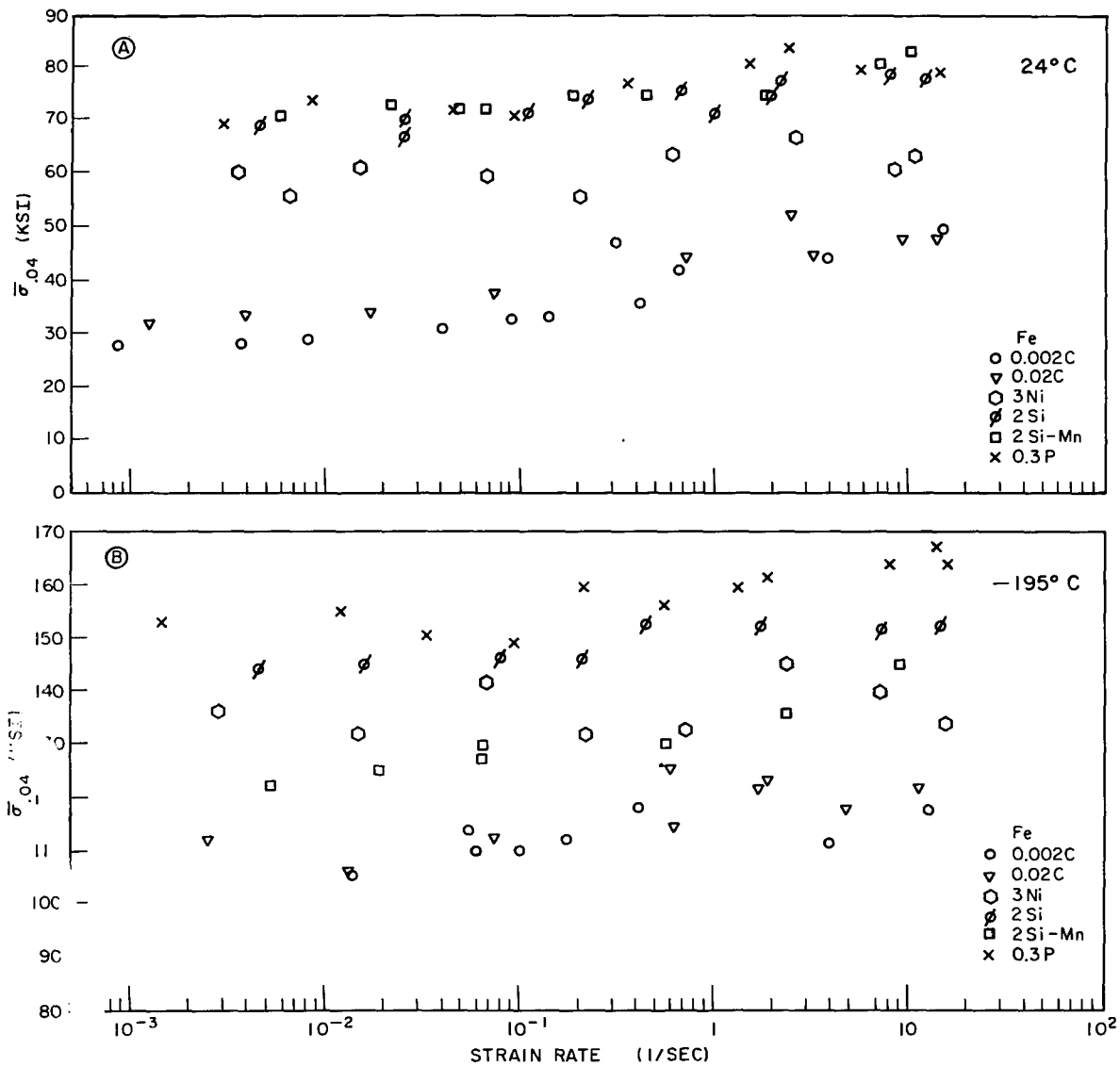

Fig. 5 - Comparison of strain-rate sensitivities of the six iron alloys at -195°C and 24°C

The large thermal component of the flow strength at -195°C caused the strengths of the alloys to increase (Fig. 5b); therefore, the effective strengthening resulting from the elements changed considerably. The phosphorus alloy became the strongest with 0.4% flow strength equal to 165 ksi at $\dot{\epsilon} = 12\ sec^{-1}$. This flow strength is 10 ksi stronger than the silicon alloy and 20 ksi stronger than the nickel alloy. A noticeable result is the change in the relative positions of the silicon-manganese and nickel alloys. The alloy containing nickel was stronger than the one containing silicon-manganese for $\dot{\epsilon} < 10\ sec^{-1}$, at -195°C, in contrast to the room-temperature behavior when the silicon-manganese alloy is the stronger over the whole strain-rate range and comparable with the silicon and phosphorus alloys.

THE TEMPERATURE DEPENDENCE OF THE FLOW STRESS

In the temperature range +177°C to -195°C the flow stresses of the alloys were measured at $\dot{\epsilon} = 2\ sec^{-1}$ in the following conditions: (a) water quenched and stored in liquid nitrogen prior to testing, (b) water quenched and aged 3 months at room temperature, and (c) furnace cooled, with all three treatments following the recrystallizing anneal.

For temperatures above 54°C the strength of the 0.002% C iron was independent of the thermal history and athermal between 121° and 177°C, but below 54°C the aged alloy was the strongest, Fig. 6a. In all conditions the strengths increased as the temperature decreased; the only anomaly occurred between 38°C and 24°C, where the strength of the quenched iron was marginally less than the furnace-cooled one. Such a small difference, 2 ksi, obtained in isolation would normally be neglected, but softening, when carbon was retained in solution, was a feature common to several systems.

With the 0.02% C iron the effect of twinning is apparent in the flow curves of the aged and furnace-cooled material; the curves show a marked reduction in slopes at the lower temperatures, Fig. 6b. In contrast, the quenched alloy suffered no reduction in slope and, though it twinned, was stronger than the aged alloy at -195°C. Softening is observed in the quenched alloy, with the furnace-cooled state being stronger than the quenched between -100° and 24°C.

When silicon was added, the quenched state was always stronger than the furnace cooled and increases of 25 to 35 ksi were obtained by aging (Fig. 6c). When silicon and manganese were present together, the reduction in alloy strength and drop in the temperature dependence of the quenched-alloy strength between -73° and 38°C caused the furnace-cooled alloy to become stronger than the quenched at -29°C (Fig. 6d). The latter result showed again that interstitial carbon can reduce the strength of the alloy over a limited temperature range.

Nickel and phosphorus additions produced changes similar to those of silicon. The flow strengths of the alloys containing nickel and phosphorus had a strong temperature dependence, and the aged and furnace-cooled states possessed the highest and lowest strengths, respectively, Figs. 6e and 6f. Above 24°C the quenched nickel alloy was the only one to age significantly during the test and to have strengths greater than at the ambient.

A comparison of the temperature dependence of the alloys after quenching is shown in Fig. 7a. In the range 18°C to -140°C the strength of the 0.02% C iron is less than that of the 0.002% C iron. Similarly, manganese reduces the strength of the silicon alloy at all temperatures, and the differing temperature dependences change the effectiveness of the additions as strengtheners. This is evident in the phosphorus-iron alloy. At 121°C its strength is less than that of the silicon and silicon-manganese alloys, but at -18°C, it becomes stronger than the silicon-manganese and at -195°C it becomes stronger than the silicon iron.

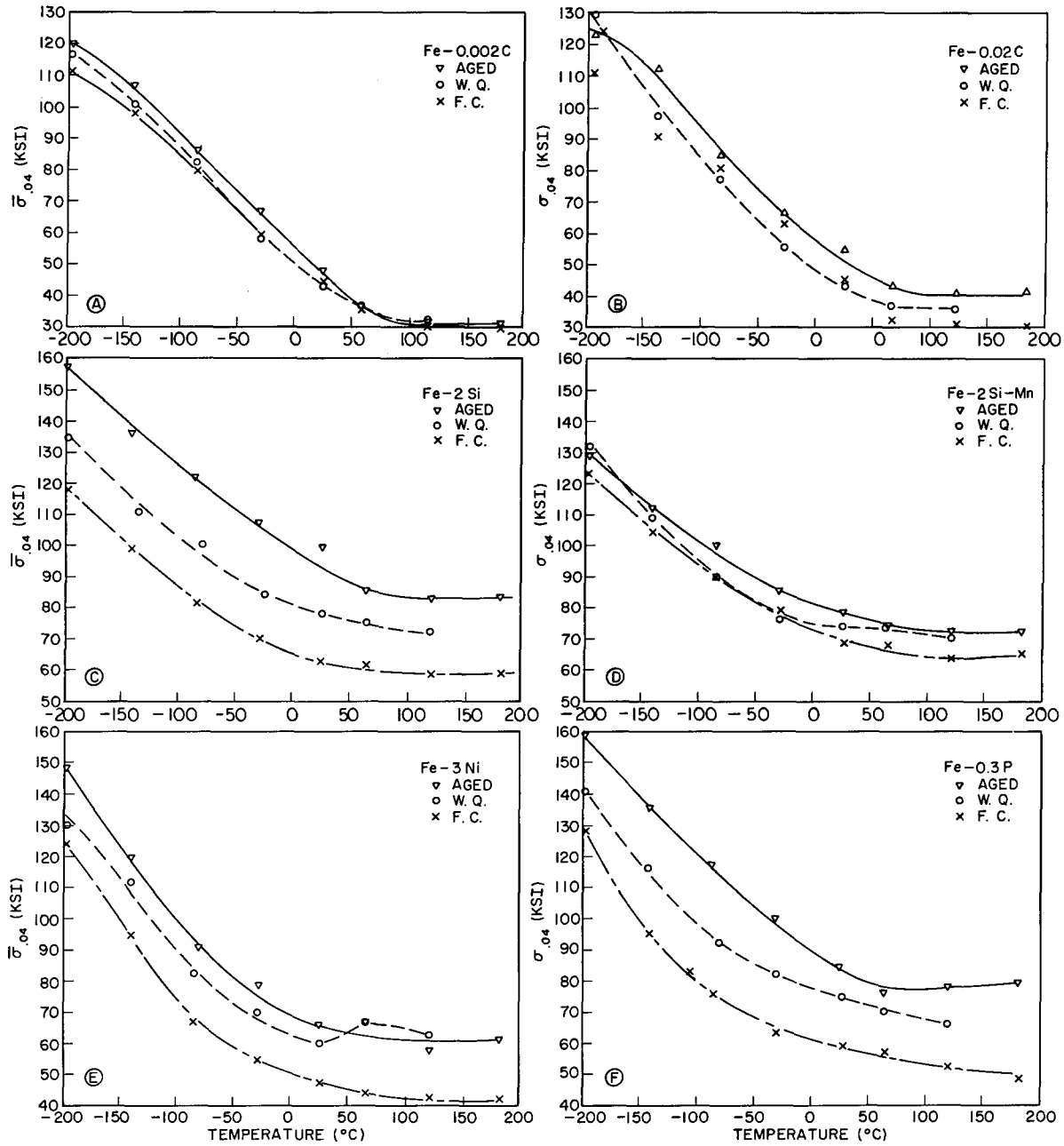

Fig. 6 - Temperature sensitivity of the strength of the six iron alloys at a strain rate of 2.0 sec^{-1}

After furnace cooling, the carbon was disposed as carbides along the grain boundaries, providing negligible strengthening. Therefore, the silicon-manganese alloy was stronger in the furnace-cooled state, in contrast to the quenched state where manganese had a softening effect in the presence of carbon (Fig. 7b).

A feature of the furnace-cooled state was the softening produced by the phosphorus and nickel additions. Nickel had the greater effect, reducing the strength of the iron alloy by as much as 10 ksi. The softening occurred in the range 4°C to -157°C, while the softening effect of phosphorus was less and restricted to the range -51°C to -140°C.

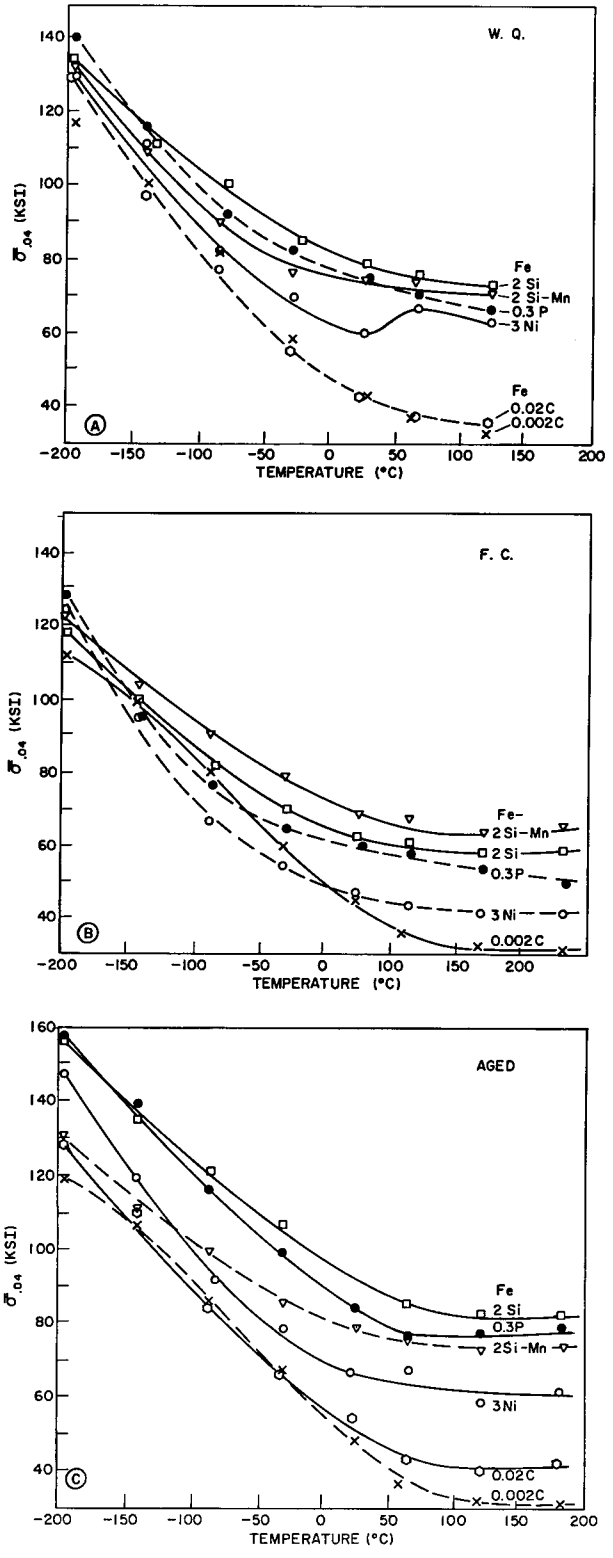

Fig. 7 - Comparison of the temperature dependence of the strength for the six iron alloys after (a) water quenching, (b) furnace cooling, (c) quenching and aging 3 months; at a strain rate of 2.0 sec^{-1}

When quenched and aged, the silicon alloy was the strongest above -140°C, with the phosphorus iron having similar strength at -195°C, Fig. 7c. Since the temperature dependences of the strength differed, the relative strengthening of the alloy additions varied, but it is evident that the strengthening effects of the elements at room temperature cannot be used as a guide to their behavior at lower temperatures.

DISCUSSION

Effect of Strain Rate and Temperature on Flow Properties

In iron solute, additions can lead to both strengthening and softening (13,18-22), the latter being defined by Arsenault (23) as a reduction in the thermal dependent part of the strength τ^*. Softening, as represented by a reduction in the engineering strength, is considered first in relation to the present results. Other bcc alloy systems have shown solution softening (24-27) the actual effect depending on the strain rate, temperature, and thermal history. The explanation of the softening is still controversial because of the difficulties encountered in obtaining interstitial free alloys and because of the assumptions made in the models. In relation to alloy-softening studies the present investigation is insufficiently controlled to provide data for critically evaluating the appropriate flow model. Discussions by Conrad (28) and Stein (29) suggest that a consensus on an operative model has not yet been arrived at. However, once agreement is reached on a model, its application will depend on its relevance to technologically interesting alloys. The present alloys do not satisfy the latter requirement either, but since they represent an increasing complexity, they are valuable for assessing the usefulness of the currently available models.

When tested at conventional strain rates, the strengthening due to interstitial carbon can be expressed as a function of $c^{1/2}$ (30,31), $c^{1/3}$ (32), or c^{-1} (33), depending on the model used, where c is the weight percent of carbon. For conditions deviating from the above, less confidence can be placed in this type of relationship, and the present results show that strengthening by carbon relies considerably on the combination of elements present and the test conditions.

Leslie et al. (13) used a titanium addition to "getter" the interstitials and render them ineffectual in their strain-rate sensitivity studies of iron alloys. However, the differences between the present 0.002% C iron flow stresses and their data are negligible and show that at these carbon levels the strain-rate sensitivity is insensitive to the interstitial level. Similarly, although the initial strengths of the nickel and silicon alloys are greater, the strain-rate sensitivities are similar to those of the titanium-gettered alloys.

With the exception of the silicon-manganese alloy, the strain-rate sensitivities at -195°C were less than those at room temperature, and, compared over the strain-rate range, the phosphorus, silicon, and carbon irons have similar sensitivities. This, however, is misleading, because the strengths of the two alloy irons are essentially independent of $\dot{\epsilon}$ in the range 10^{-3} to 10^{-1} and 1 to 10 sec^{-1} but are strongly sensitive in the range 10^{-1} to 1 sec^{-1}. Difficulties also exist in relating the strain-rate sensitivity of the nickel iron to some monotonic law because of the fluctuations obtained. In the majority of investigations, difficulties in reproducing strain rate have lead to some scatter, but the fitting of smoothed curves to the data has shown a steady increase in strength with strain rate. An alternative to this interpretation is suggested by Krafft et al. (9) and Hettche (17). In a voluminous series of tests these investigators found that statistically reproducible changes in flow stress occur with $\dot{\epsilon}$; this observation was described as "strain rate spectrum." Whether the present results can be interpreted similarly is doubtful because of the limited number of tests, but a curve smoothing out the variations cannot be drawn in view of their results.

The strong temperature dependence characteristic of bcc metal is shown in Figs. 6 and 7. The aged alloys possess the highest strengths at temperatures above -195°C, except for the 0.02% C and 2% silicon-1% manganese alloys where the strength after aging

is exceeded by the quenched-material strength at -195°C. In the 0.02% C iron extensive twinning causes this change in the relative position. No similar discontinuity is seen in the silicon-manganese flow curves to indicate that deformation by twinning has increased rapidly, though as observed in the micrographs and thin foils, deformation at -195°C involved both slip and twinning in all alloys.

The interstitial carbon strengthening depended on the temperature, strain rate, and the associated elements. When carbon was present with silicon, nickel, or phosphorus, the strength of the quenched alloy was stronger than the furnace-cooled state at all temperatures. In the furnace-cooled state the major part of the carbon was out of solution and in the form of coarsely distributed carbides. For the 0.002% C alloy, the difference in the carbon contents between the quenched and furnace-cooled matrixes was small but sufficient to reduce the strength of the quenched alloy between 24°C and -46°C. More substantial softening occurred when the soluble carbon content was increased, and in the range 24°C to -101°C, the furnace-cooled 0.02% C alloy was as much as 10 ksi stronger than the quenched alloy.

Limited softening arising from the carbon in solution was also found in the silicon-manganese alloy. In this alloy the strength in the quenched state was less temperature sensitive between -18°C and 121°C than in the furnace-cooled alloy. The quenched alloy was stronger at -195°C and 121°C, but it was slightly less at -29°C. Carbon also modified the strengthening effect of manganese when present with silicon. In the quenched state manganese reduced the strength of the silicon alloy, whereas when the carbon was precipitated after furnace cooling, the strengthening due to manganese in solution became apparent and the silicon-manganese alloy was stronger than the silicon alloy. The softening is due to either the carbon or the manganese, acting separately or interdependently, with the latter appearing most probable. Although manganese produces softening in pure iron (13), manganese increased the strength of the silicon alloy when the major portion of carbon was out of solution. This latter result is contrary to softening produced by manganese in iron and suggests further solute interaction.

Softening effects were also found with the phosphorus and nickel alloys. Nickel softens in a range similar to that found by Leslie et al. (13), which indicates that the softening is not affected by the remaining interstitials. These results, together with those for the carbon-iron and the silicon-manganese alloys, emphasize the complex nature of softening and the difficulties in interpreting the combined effect of elements in terms of their individual behavior.

Temperature Dependence of Thermal Strengthening

When studying the temperature dependence of the strength (τ), it is beneficial to separate the shear strength into its thermal (τ^*) and athermal (τ_A) components, where

$$\tau = \tau^* + \tau_A.$$

The thermal component is a short-range effect acting over several atomic spacings, and the athermal component is due to the strengthening arising from solute, precipitate, and dislocation-dislocation interactions. More recently some discussion has centered around the "athermal" nature of interstitial and solute strengthening, and the results of several workers indicate that interstitials may contribute a large thermal strengthening component (20,24,34). Further comment on the interstitial strengthening is made subsequently, but the first step is to distinguish between the thermal and athermal strengthening components. It was assumed in determining τ^* that the strength was athermal at an $\dot{\epsilon} \approx 2$ sec^{-1} when the strength was the same as that obtained at an $\dot{\epsilon}$ of 10^{-4} sec^{-1}; the results for τ^* are shown in Figs. 8a through 8e.

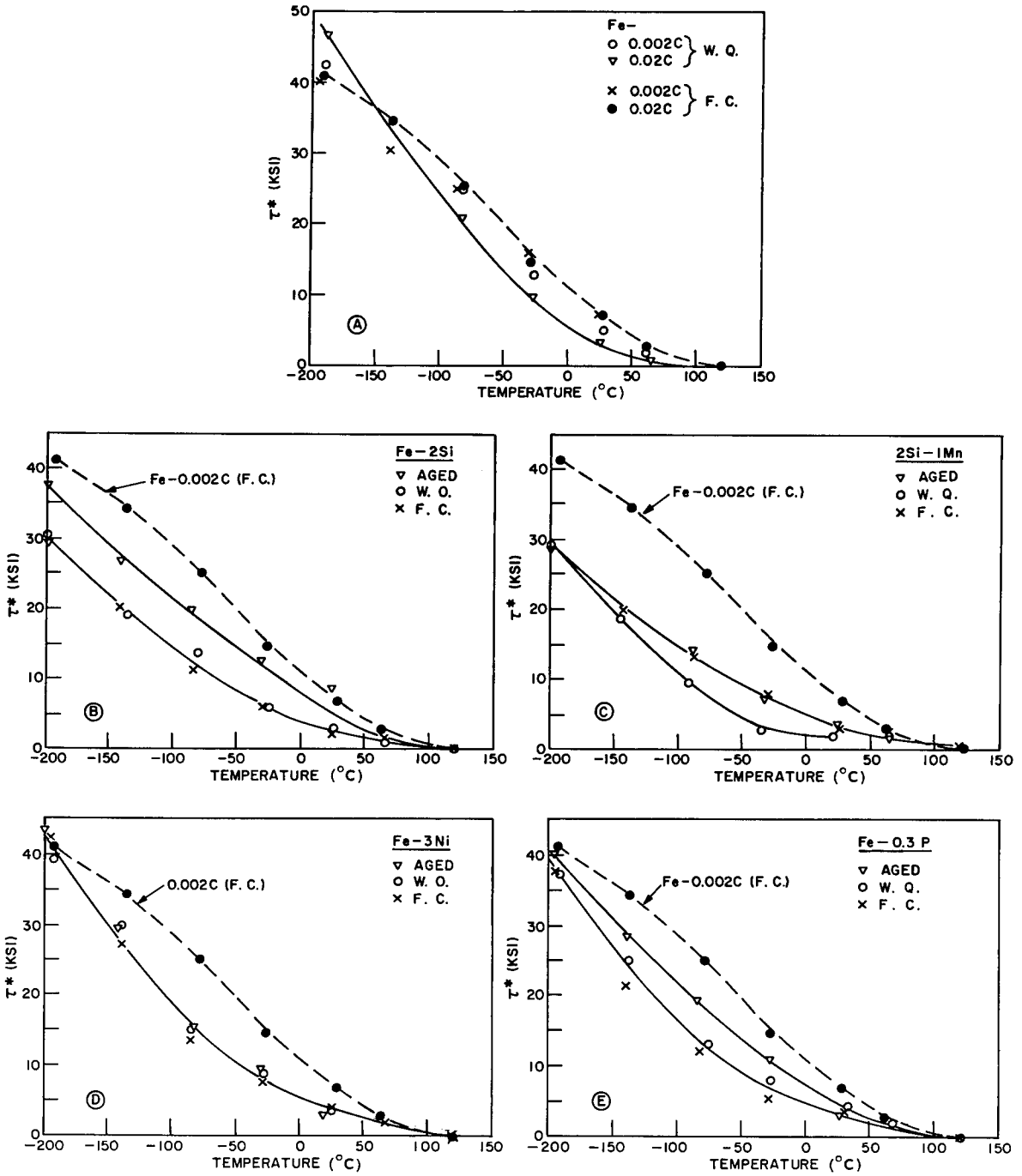

Fig. 8 - The temperature dependence of the thermal strengthening components for the six iron alloys

The temperature dependence of τ^* for the quenched 0.002% C iron was less than that for the furnace-cooled condition and was further reduced when the carbon retained in solution was increased to 0.02% C (Fig. 8a). Once the carbon in the 0.02% C alloy was precipitated by furnace cooling, τ^* became similar to that for the furnace-cooled 0.002% C iron, indicating that the equilibrium carbon contents in the ferrite were much the same. Similarly, Lahiri and Fine (35) found in iron-copper alloys that once the ϵ copper precipitated the original temperature dependence of iron was regained. The change in temperature dependence observed is in contrast to that found by Stein and Low (34), where the τ^* decreased on reducing the carbon from 44 to 0.005 ppm, but Tanaka and Conrad (22) have reported that carbon can reduce the temperature dependence of iron, and a number of studies have found softening due to interstitial nitrogen (19,36).

The temperature dependence of τ^* for the quenched and furnace-cooled states was the same for the silicon, nickel, and phosphorus alloys, Figs. 8b, 8d, and 8e, any softening effect due to the carbon being suppressed by these additions. Once the alloys were aged, the coherent carbides which precipitated in the former two alloys increased the τ^*. If the strain fields associated with the carbides were responsible for the modified temperature dependence, the original temperature dependence should be regained once the strain fields disappear. Such a result was obtained with the incoherent particles in the nickel alloy when the temperature dependence of τ^* was independent of the heat treatments, Fig. 8d. With manganese and silicon present together (Fig. 8c), carbon reduced the τ^* dependence of the furnace-cooled alloy in a fashion similar to the reduction in the iron-carbon alloys. On aging the silicon-manganese alloy, the temperature dependence of τ^* of the furnace-cooled state was regained, indicating that the matrix strain around the precipitated carbides was small.

The effect of these additions on τ^* can be summarized as follows by using the furnace-cooled alloy as the reference state:

1. The temperature dependence of τ^* is reduced by carbon in solution for the iron-carbon and silicon-manganese alloys.
2. The temperature dependence of τ^* is unaffected by carbon in solution for the silicon, nickel, and phosphorus alloys.
3. The temperature dependence of τ^* is increased by aging for the silicon and phosphorus alloys.
4. The temperature dependence of τ^* is unaffected by aging the nickel alloy.

Two distinct explanations for the softening have been developed. One model formulated by Dorn and coworkers (37,38) suggests that deformation at low temperatures is controlled by the nucleation of a double kink, while another proposed by Ravi and Gibala (24,25) considers that the interstitials and substitutional solute aggregates are responsible for the temperature dependence and the softening. In the model proposed by Dorn and coworkers the low-temperature deformation relies on moving the dislocation, under the combined action of the applied stress and thermal energy, from its low energy position over the energy barrier by the formation of a double kink. At 0°K the thermal contribution is zero, and the stress applied must exceed the intrinsic strength of the lattice, the Peierls strength (τ_p). This model gives the temperature dependence of the shear stress (τ^*) as

$$\tau^*/\tau_p = f(U_n/2U_k) \approx f(T/T_c),$$

where, U_n is the thermal energy necessary to nucleate a pair of kinks, U_k is the energy of an isolated kink, and T_c is the temperature at which the strength becomes independent of temperature.

To test whether this particular model is applicable to the flow data, the $\tau^*_{0°K}$ value was first obtained by extrapolating the flow curve to 0°K; the results are given in Table 2.

The $\tau^*_{0°K}$ value of 64 ksi for the furnace-cooled 0.002% C iron compared with values of 45 and 63 ksi obtained by Spitzig and Keh (39) for slip on {110} and {112} iron single crystals, respectively. The nickel alloy $\tau^*_{0°K}$ value of ≈ 63 ksi obtained by extrapolation compares favorably with a value of ≈ 70 ksi obtained in Gamble's (21) work. The temperature T_c was obtained numerically by fitting the experimental results to the theoretical curves at 77°K.

Compared with the theoretical curves (37,38) for $\alpha = 1$ and $\alpha = 0$, where the parameter α characterizes the energy profile to be surmounted, the data for the six alloys in the three conditions fit reasonably well for $T/T_c < 0.6$, Fig. 9. Whether the deviation is significant depends on the accuracy of the energy profile characterization. Smidt (40) found that the data for pure iron also deviated from the predicted curves, but he fitted his data to an empirical curve $T/T_c = [1 - \sqrt{(\tau^*/\tau_p)}]$, which also fits the present data. In view of the agreement with Smidt's curve for iron, similar deformation processes are expected to occur in the current alloy series. Assuming that the resolution of the method is adequate, the presence of solutes or precipitate particles has little effect on the deformation mechanisms at low temperatures.

Table 2
Thermal Component of the Strength at 0°K and Critical Temperatures (T_c)

Alloy	$\tau^*_{0°K}$ (ksi)			T_c (°K)·Calculated			T_c (°K) Experimental
	Furnace Cooled	Quenched	Aged	Furnace Cooled	Quenched	Aged	
Fe-0.002 C	64	71	64	445	—	—	390 - 450
Fe-0.02 C	64	72	65	—	445	—	390 - 450
Fe-2 Si	45	45	51	405	405	494	390 - 450
Fe-2 Si-1 Mn	44	48	44	405	—	405	300 - 400
Fe-3 Ni	63	63	63	405	405	405	390 - 450
Fe-P	60	60	58	445	445	445	400 - 450

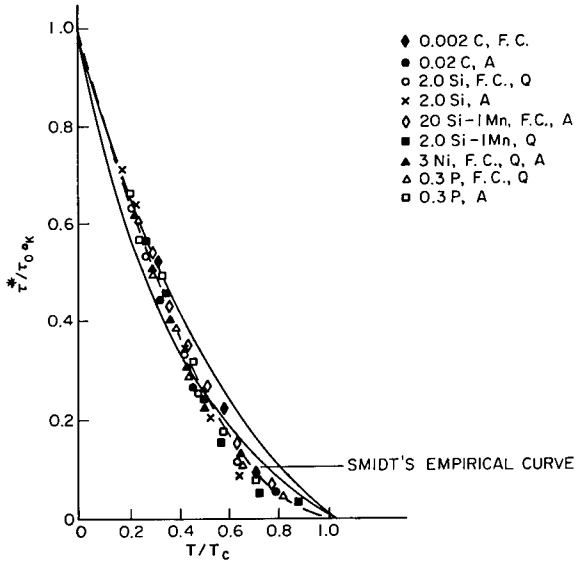

Fig. 9 - A comparison of the $\tau^*/\tau_{0°K}$ vs T/T_c with the theoretical predictions of Dorn and Rajnak (37) and Smidt's (40) empirical relation

In previous studies of the iron-nickel alloys the softening has been attributed to reductions in $\tau^*_{0^\circ K}$, but the present results show that values of $\tau^*_{0^\circ K}$ for the furnace-cooled irons, though less than the values normally found for pure iron (40), are little altered by the nickel and phosphorus additions. In contrast, the reduced temperature dependence for the silicon and silicon-manganese alloys is accompanied by a lower $\tau^*_{0^\circ K}$, which is consistent with the predicted changes, but it is evident that, considered as a group, the reduction in $\tau^*_{0^\circ K}$ by itself is not the sole prerequisite for softening.

An alternative explanation for softening is that τ^* is reduced when the preexponential function γ_0 is reduced. The strength τ^* is then given by

$$\tau^* = \frac{\Delta G - K \ln \gamma_0/\dot{\gamma}}{\nu},$$

where ΔG is the free energy, ν is the frequency factor, and $\dot{\gamma}$ is the shear-strain rate. The preexponential factor γ_0 is proportional to ρVAb, where ρ is the mobile dislocation density, b is the Burgers vector, and A is the area swept out. A change in this factor by an increased mobile density was considered responsible for the softening in the iron-nickel alloy by Nakada and Keh (19). Their principal objections to the softening caused by a reduction in the Peierls stress were that 0.04 at -% nitrogen was too small to alter the latter significantly and that the nitrogen affected the temperature dependence of τ^*, an observation similar to that found in the current data. Also the reduction in τ^* was found to be insensitive to the nitrogen content in contrast to the influence of carbon.

Christ and Smith (36) also studied the softening in iron-nitrogen alloys and proposed that the softening was due to the interstitials producing an elastic dipole distortion which facilitates cross slip. By this impurity-induced cross-slip process the authors predicted softening in iron-carbon systems when the solute content is in the range 0.04 to 0.06 at -% and the carbon dispersed randomly, with no finely dispersed phases present. The current test conditions satisfy the Christ and Smith stipulations and the model appears to be pertinent to the softening obtained. Christ and Smith also considered that the presence of the second phase reduced the temperature dependence of τ^*, but this was not observed in the aged nickel alloy, when the particles were incoherent. In the alloys containing coherent or partially coherent particles, τ^* was actually increased.

In Ravi's and Gibala's (24,25) explanation of solute softening, an intrinsic lattice strength is not assumed because the authors consider that the available data are from insufficiently pure materials and that the indications are for $\tau^*_{0^\circ K}$ to decrease with purification. A further objection to the lattice possessing an inherent strength or a change in the mobile dislocation density being responsible for the softening is that the softening phenomena is not reversible. To illustrate this irreversibility of the softening, the authors (24,25) show that in the niobium-oxygen system softening occurs when oxygen is added to purified niobium but not if an alloy of similar composition is obtained by purifying niobium.

Softening is expected when interstitials are scavenged by substitutional elements which readily form carbides or nitrides. For alloy systems, where compound formation is improbable, Ravi and Gibala (24,25) proposed, on the basis of internal friction, field ion microscopy, and thermodynamic results, that interstitial and substitutional elements associate. Softening occurs by changing a random solution to one containing associated solutes, which reduces the number of obstacles to dislocation movement and reduces the total free energy of the solution. The effective hardening of an associated solute is less than that of the unassociated solute atom.

Softening, defined as a reduction in τ^* of the furnace-cooled 0.002% C iron was obtained for all the quenched alloys. The quenched alloys were stored in liquid nitrogen to minimize clustering and carbide formation. Whether any association occurred during the quench was not ascertained, but the agreement with the prediction of Christ and Smith (36) for randomly

disposed interstitials suggests that little clustering occurred. Further, the presence of the interstitials had no effect on τ^* for the nickel-phosphorus and silicon alloys. If the softening depends on the substitutional/interstitial solutes ratio, the quenched alloys would be expected to be softer than the furnace-cooled ones, but this was only observed in the silicon-manganese alloy and was the exception in the present data. If aggregation was responsible for softening in the iron-carbon alloys, then the absence of softening, when nickel, silicon, or phosphorus were present, indicates that only certain aggregates produce softening.

A further indication that the reduction in τ^* is not due to the aggregation of solute elements alone is the data of Lahiri and Fine (35) on iron-1.67% copper. Their results show that τ^* is reduced when the ferrite is quenched and supersaturated with copper, but after aging and precipitating ϵ copper, the original temperature dependence of the alloy is regained. If copper-copper or copper-interstitial aggregates were responsible for the softening, these would be expected to remain after aging and prevent the original τ^* from being obtained. Similarly, the temperature dependence of the quenched silicon-manganese alloy returns to that of the furnace-cooled alloy when aged to indicate that the softening was not purely the result of a permanent association of the solute and interstitials.

The alloys used in this study differed from those previously studied by the high interstitial contents and the modification of these by heat treatment, rather than purification. In the quenched and furnace-cooled states, the ferrite matrix was essentially precipitate free; therefore, the changes in the dependence of τ^* with temperature might be expected to conform with the predictions of the solute strengthening. In practice this was not found, though the softening accompanied by a reduction of $\tau^*_{0^\circ K}$ was consistent with softening produced by silicon or silicon and manganese, and increasing the interstitial content reduced τ^* for the iron-carbon alloys. The expansion of these results into generalizations applicable to all the systems was not possible and probably the most interesting result was the agreement between the softening due to carbon and the predictions of Christ and Smith (36).

CONCLUSIONS

1. The strain-rate sensitivity of iron is unaffected by 0.002% C, but is reduced by nickel, silicon, and phosphorus additions at ambient temperatures.

2. At a strain rate of 2 sec^{-1} and for limited temperatures ranges nickel, phosphorus, and carbon can produce an overall reduction in the strength of iron. In the iron-carbon alloys containing 0.002 to 0.02% C, softening increased with increasing carbon content.

3. The nickel, silicon, phosphorus, and carbon additions reduced the thermal component of the strength of the iron, which was also modified by the presence of coherent precipitates.

4. The softening due to the interstitial carbon was consistent with an impurity-induced cross-slip mechanism.

5. The deformation for the alloys in the differing heat-treated state are similar to those on pure iron in the range -195°C to 24°C.

6. The current models for softening did not satisfactorily explain the observed changes in flow properties wrought by the alloy additions and heat treatments.

ACKNOWLEDGMENTS

The authors recognize the cooperation of Mr. T. Lupton and Mr. R. Scott in facilitating the thermal processing of the alloys and Dr. J. M. Krafft for his imperturbable interest throughout the work.

REFERENCES

1. J.M. Krafft, Appl. Mat. Res. 3, 88 (1964)
2. C.J. McMahon, Acta Met. 14, 839 (1966)
3. D. Hull, Acta Met. 9, 191 (1961)
4. J.T. Barnby, Acta Met. 15, 903 (1967)
5. B.J. Brindley, Acta Met. 18, 325 (1970)
6. F.A. McClintock and A.S. Argon, eds., Mechanical Behavior of Materials, Addison-Wesley, Reading, Mass., 1966
7. A.S. Tetelman and A.J. McEvily, Jr., Fracture of Structural Materials, Wiley, New York, 1967
8. J.P. Hirth and J. Lothe, Theory of Dislocations, McGraw-Hill, New York, 1968
9. J.M. Krafft, L.R. Hettche, A.M. Sullivan, and F.J. Loss, Trans. ASME, J. Eng. Ind. 92, Series B, No. 2, 330-338, (1970)
10. W.C. Leslie and R.J. Sober, Trans. Am. Soc. Metals 60, 459 (1967)
11. J. Eftis and J.M. Krafft, Trans. ASME, Series D, 87, 257-263 (1965)
12. J.M. Krafft and G.R. Irwin, "Fracture Toughness Testing and its Applications," Am. Soc. Testing Materials Special Publication 381 (1965)
13. W.C. Leslie, R.J. Sober, S.G. Babcock, and S.J. Green, Trans. Am. Soc. Metals 62, 690 (1969)
14. K.F. Hale and D. McLean, J. Iron Steel Inst. 201, 337 (1963)
15. W.C. Leslie, Acta Met. 9, 1004 (1961)
16. M.C. Inman and H.R. Tipler, Acta Met. 6, 73 (1958)
17. L.R. Hettche, "Application of Random Process Statistics to the Rate Sensitivity of Plane Strain Fracture Toughness," Metallurgical Trans. 2, 1905 (1971)
18. W. Jolley, Trans. Met. Soc. AIME 242, 306 (1968)
19. Y. Nakada and A.S. Keh, Acta Met. 16, 903 (1968)
20. R. Burbach, B.L. Mordike, and P. Haasen, J. Iron Steel Inst. 204, 390 (1966)
21. R.P. Gamble, Materials Sci. Center Rpt. 1074, Cornell Univ, Ithaca, N.Y., Master's Thesis, 1969.
22. T. Tanaka and H. Conrad, J. Metals 21, 117A (1969) (Abstract)
23. R.J. Arsenault, Acta Met. 15, 501 (1967)
24. K.V. Ravi and R. Gibala, Scripta Met. 3, 547 (1969)
25. K.V. Ravi and R. Gibala, Acta Met. 18, 623 (1970)

26. T.E. Mitchell and P.L. Raffo, Can. J. Phys. 45, 1047 (1967)

27. P.L. Raffo and T.E. Mitchell, Trans. Met. Soc. AIME 242, 907 (1968)

28. H. Conrad, Acta Met. 15, 147 (1967)

29. D.F. Stein, Acta Met. 15, 150 (1967)

30. J.W. Christian, I.S.I. Special Rept. 93, p. 1 (1965)

31. W.S. Owen, E.A. Wilson, and T. Bell, High-Strength Materials, V.F. Zackay, ed., Wiley, New York, 1965, p. 167

32. P.G. Winchell and M. Cohen, Trans. Am. Soc. Metals 55, 347 (1962)

33. G. Schoeck and A. Seeger, Acta Met. 7, 469 (1959)

34. D.F. Stein and J.R. Low, Jr., Acta Met. 14, 1183 (1966)

35. S.K. Lahiri and M.E. Fine, Trans. Met. Soc. AIME 1, 827 (1970)

36. B.V. Christ and G.V. Smith, Trans. Met. Soc. AIME 1, 827 (1970)

37. J.E. Dorn and S. Rajnak, Trans. Met. Soc. AIME 230, 1052 (1964)

38. P. Guyot and J.E. Dorn, Can. J. Phys. 45, 983 (1967)

39. W.A. Spitzig and A.S. Keh, Acta. Met. 18, 611 (1970)

40. F.A. Smidt, Jr., Acta Met. 17, 381 (1969)

Appendix

DETERMINATION OF THE TENSILE INSTABILITY STRAIN FROM COMPRESSION STRESS-STRAIN CURVE

To determine the tensile instability strain from compression data, the true stress ($\bar{\sigma}$) versus true strain ($\bar{\epsilon}$) curves must be assumed to have identical shapes in tension and compression; i.e., if

$$\bar{\sigma}_{TEN} = f_T(\bar{\epsilon}_T)$$

$$\bar{\sigma}_{COM} = f_c(\bar{\epsilon}_c),$$

then

$$f_T(\bar{\epsilon}_T) = -f_c(-\bar{\epsilon}_T).$$

Several investigators* have demonstrated the validity of this assumption for a variety of alloys. It can also be argued that dislocation motion is caused by shear stresses on operative slip planes. Since a change from compression to tension loading produces a change in sign in the shear stress, the strain-rate and temperature sensitivity of the flow properties should be similar in compression and tension.

An important consideration in making the transformation from compression to tension curve, however, is to compensate for barreling of the compression specimen from friction end effects. Such effects cause a nonuniform deformation of the specimen and are minimized, but not eliminated, by lubricating the contact surfaces with powder Teflon. It is reasoned that the deformation is most uniform (uniaxial) at the midsection of the plug; therefore, the ratio of diametrical (ϵ_d) to longitudinal (ϵ_ℓ) strain provides a measure of barreling correction. A theoretical relationship between ϵ_d and ϵ_ℓ can be obtained by neglecting elastic strains and invoking the consistency of volume for plastic deformation. It follows

$$\text{Initial (area} \times \text{length)} = \text{Final (area} \times \text{length)}$$

$$A_0 = \ell_0 = A \times \ell$$

$$\left(\frac{\ell_0 + \Delta\ell}{\ell_0}\right)\left(\frac{r_0 + \Delta r}{r_0}\right)^2 = 1$$

$$(1 + \epsilon_\ell)(1 + \epsilon_d)^2 = 1.$$

This relation is shown on a $\epsilon_\ell/2\epsilon_d$ versus ϵ_ℓ plot in Fig. A1 along with experimental points for a variety of steels. The ϵ_d and ϵ_ℓ data were determined by measuring the permanent change in length and diameter of the compression specimen (7/16 in. long $\times$ 1/4 in. diameter) with a Vernier micrometer. The slope of the data is seen to follow the theoretical relationship while the decrease in $\epsilon_\ell/2\epsilon_d$ ratio is attributed to frictional effects. The trend line is fitted to the experimental data,

*W.C. Leslie and R.J. Sober, Trans. Am. Soc. Metals 60, 459 (1967); A.B. Watts and H. Ford, Proc. Inst. Mech. Eng. 169, 1141-1149 (1955)

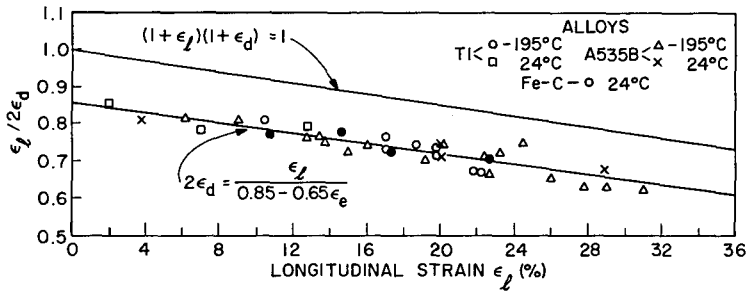

Fig. A1 - The longitudinal strain-diametral strains relationship showing the empirically devised correction for barreling

$$2\epsilon_d = \frac{\epsilon_\ell}{0.85 - 0.68\epsilon_\ell}$$

and is used to convert the longitudinal (ϵ_ℓ) to true longitudinal strain ($\bar{\epsilon}_\ell$)

$$\ln(\epsilon_d + 1) = \bar{\epsilon}_d = 1/2\ \bar{\epsilon}_\ell.$$

Given the true stress-strain curve, the tensile instability strain must still be determined. From elementary strength of materials, the instability strain (ϵ_c) is defined as that strain where

$$d\bar{\sigma}/d\bar{\epsilon} = \bar{\sigma}.$$

Another form for the instability criterion is

$$d\bar{\sigma}/d\epsilon_T = \bar{\sigma}/(1 + \epsilon_T),$$

where ϵ_T is the tensile engineering strain. This result* allows a convenient geometrical construction for determining ϵ_c. As illustrated in Fig. A2, a line drawn from $\epsilon = 1$ on the strain axis and tangent to the stress-strain curve defines a slope of $\bar{\sigma}/(1 + \epsilon_T)$. By the above equation, the point of tangency also defines the instability strain.

To summarize, the following steps are used to reduce the flow data:

1. The isothermal stress-strain curve is obtained by recording the total strain after each compression step with the subsequent yield stress.

2. The diametrical strain is determined by the empirical relationship

$$2\epsilon_d = \frac{\epsilon_\ell}{0.85 - 68\epsilon_\ell},$$

which corrects for end effects.

3. The true stress versus tensile (engineering) strain relationship is determined from the identities

$$\bar{\epsilon}_T = 2\bar{\epsilon}_d = 2 \ln(\epsilon_d + 1)$$

*A. Nádai, Theory of Flow and Fracture of Solids, 2nd ed., McGraw-Hill, New York, 1950, p. 71

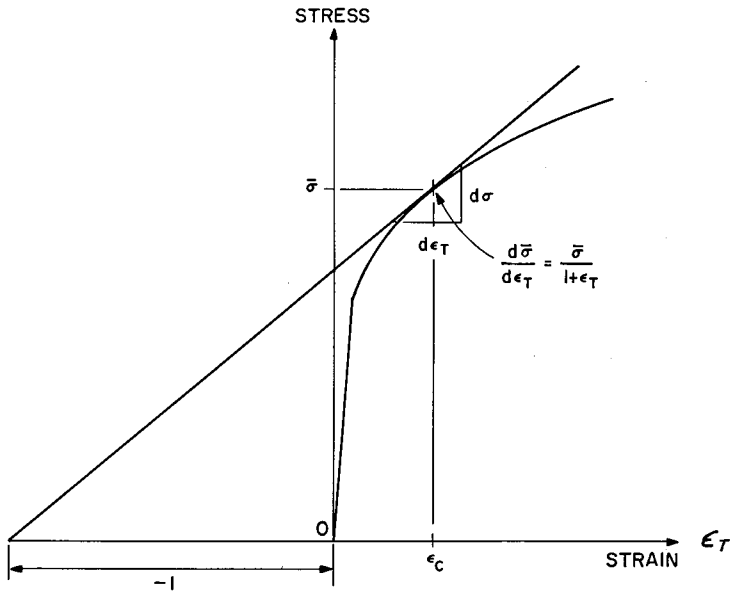

Fig. A2 - Considére construction for determining instability strain from true stress-tensile strain curve

$$\epsilon_T = e^{\bar{\epsilon}_T} - 1$$

and

$$\bar{\sigma} = \sigma_c (1 + \epsilon_\ell)$$

4. The instability strain is determined from the Considére construction, Fig. A2, and the instability strain versus temperature for the six alloys are shown in Fig. A3.

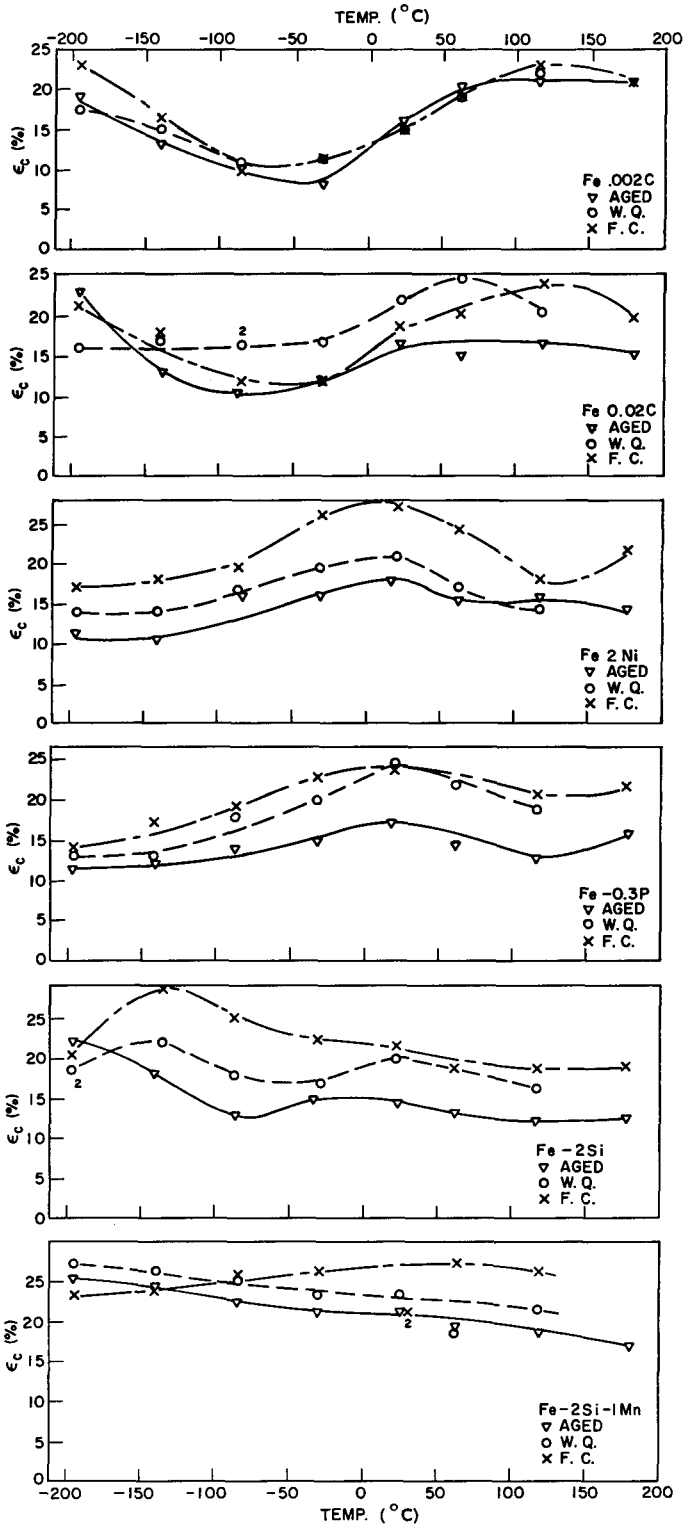

Fig. A3 - Instability strains versus temperature for the six iron alloys obtained at a strain rate of 2.0 sec^{-1}